

Steady-state bubbles beyond local thermal equilibrium

Tomasz Krajewski,¹ Marek Lewicki,² Ignacy Nałęcz² and Mateusz Zych²

¹*Nicolaus Copernicus Astronomical Center of the Polish Academy of Sciences, ul. Bartycka 18, 00-716 Warsaw, Poland*

²*Faculty of Physics, University of Warsaw, ul. Pasteura 5, 02-093 Warsaw, Poland*

E-mail: tkrajewski@camk.edu.pl, marek.lewicki@fuw.edu.pl,
ignacy.nalecz@fuw.edu.pl, mateusz.zych@fuw.edu.pl

ABSTRACT: We investigate the hydrodynamic solutions for expanding bubbles in cosmological first-order phase transitions going beyond local thermal equilibrium approximation. Under the assumption of a tangential field profile, we supplement the matching conditions with the entropy produced due to the interaction of the bubble wall with ambient plasma. This allows us to analytically compute the corresponding fluid profiles and find bubble-wall velocity. We show that due to the entropy production, two stable solutions corresponding to a deflagration or hybrid and a detonation can coexist. Finally, we use numerical real-time simulations of bubble growth to show that in such cases it is typically the faster detonation solution which is realised. This effect can be explained in terms of the fluid profile not being fully formed into the predicted steady-state solution as the wall accelerates past this slower solution.

Contents

1	Introduction	1
2	Cosmological first-order phase transition parameters	3
3	Matching conditions beyond local thermal equilibrium	4
3.1	Stationary bubble-walls	4
3.2	Third matching condition	4
3.3	Entropy production details	5
4	Analytical results	6
5	Hydrodynamic simulations	8
6	Numerical results	9
7	Conclusions	11
A	Field profile widths	12
A.1	Equation for steady profiles	12
A.2	Approximate solutions for profile width	13
A.3	Comparison with simulation results	14

1 Introduction

Cosmological first-order phase transitions are a common feature in many particle-physics models. They are motivated by the possibility of realising electroweak baryogenesis [1–4] and they are capable of producing an observable background of gravitational waves [5–10]. These prospects, however, depend crucially on the dynamics of the transition. While most of the thermodynamic parameters describing the transition are fairly well understood, the computation of the wall velocity, despite recent progress [11–20], remains an issue.

It was recently shown that in the local thermal equilibrium (LTE) approximation it is possible to determine the bubble wall velocity in a steady state in a relatively simple way [12, 13, 16]. The method is based on the conservation of entropy and provides the additional matching equation relating its value across the bubble wall. Since additional friction can only slow down the wall, the resulting velocity can be interpreted as the upper bound on the full out-of-equilibrium computation. It was also demonstrated, using the example of a scalar singlet extension of the Standard Model, that non-equilibrium corrections are typically subdominant [15].

Nevertheless, this extremely useful method, similarly to all steady-state results does not take into account the dynamical formation of the heated fluid shell, which is the source of hydrodynamic obstruction. In the recent paper [21] we have shown that majority of deflagration and hybrid solutions predicted by the LTE matching equations are not realized in dynamical simulations and that real-time evolution towards deflagration/hybrid requires fine-tuning of the nucleation temperature T_n to be very close to the critical temperature $T_n \approx T_c$, i.e. the one at which the initial and final vacua are degenerate.

In this paper we generalise the matching method going beyond the LTE approximation. We obtain a new version of the third matching condition by introducing the entropy production rate. Assuming a particular class of interactions between the wall and the plasma valid for the SM and many of its extensions [22, 23], we express this rate in the thin wall regime using basic physical quantities and the effective friction parameter η [24].

The rate at which entropy is generated in the field-plasma interaction critically depends on the stationary field profile during the transition and in particular its width. Surprisingly, in the hydrodynamic lattice simulations, we find this width to be independent of friction, which allows us to estimate it using only the information stored in the effective potential. The resulting analytical field profiles are then used to compute the entropy source necessary to obtain the steady-state fluid profile in the corresponding model.

Intriguingly, our new formalism typically predicts an additional branch of stable detonation solutions. This branch of solutions is well visible in numerical simulations, continuously going to runaways with $v_w = 1$ in the limit of vanishing η . The presence of this branch gives a convenient selection rule to distinguish between physical and unphysical deflagration/hybrid solutions as it is typically the faster detonation solution which is dynamically realised. This is associated with the fact that the steady state profile predicted analytically is not fully formed as the developing solution accelerates past the velocity corresponding to the slower solution [21].

We supplement our paper with a code snippet written in Python that can determine the stationary wall velocity for both detonations and deflagrations/hybrids beyond LTE [25]. Our code is essentially a modified version of the program published in [16]. The wall velocity is computed based on parameter encoding dissipative friction and the parameters used for calculating v_w in LTE that are readily derived from the effective potential. We tested our algorithm by comparing its predictions with the results of hydrodynamic lattice simulations [26] and found that in a heartbeat it can correctly reproduce the stationary velocity to great accuracy.

The paper is organized as follows. In Section 2, we recall basic parameters describing cosmological first-order phase transitions. In Section 3, after the brief discussion of stationary profiles, we derive and generalize the third matching condition beyond the local thermal equilibrium approximation. We focus on the particular form of the entropy current widely used in the literature [24, 27], however our results are easy to adjust for alternative expressions. Then, using the new condition in Section 4, we discuss model-independent results for the wall velocity beyond the local thermal equilibrium approximation. Section 5 presents setup of the real-time hydrodynamic simulations used to verify the analytical solutions, while in Section 6 we show the results of the simulations for two representative

benchmarks, comparing them with our analytical estimates. Appendix A is devoted to discuss different approximations of the bubble-wall width, which appears in the third matching condition beyond LTE limit.

2 Cosmological first-order phase transition parameters

Cosmological first-order phase transitions (FOPTs) proceed via nucleation of bubbles containing energetically favourable phase in the background of the metastable phase. The tunnelling probability per unit time and volume at temperature T is given with [28–31]

$$\Gamma(T) = A(T)e^{-S}, \quad (2.1)$$

where for finite temperatures the Euclidean action $S = \frac{S_3}{T}$ and $A(T) = T^4 \left(\frac{S_3}{2\pi T}\right)^{\frac{3}{2}}$. Nucleation temperature is defined as the value such that the probability of a true vacuum bubble forming within a horizon radius is close to unity [32], i.e.

$$N(T_n) = \int_{T_n}^{T_c} \frac{dT}{T} \frac{\Gamma(T)}{H(T)^4} \approx 1, \quad (2.2)$$

with the critical temperature T_c representing the value at which both minima of the model-dependent effective potential are equally deep. Assuming that the transition is sufficiently fast, one can neglect the background evolution of the Universe assuming $H(t) \approx \text{const}$. Then, eq. (2.2) becomes

$$\frac{S_3}{T_n} \approx 4 \log \left(\frac{T_n}{H} \right), \quad (2.3)$$

which at the electroweak scale gives $S_3/T_n \approx 140$ [6].

In the standard hydrodynamic approximation [33, 34], it is assumed that the cosmic plasma can be modelled as the relativistic perfect fluid, with the energy-momentum tensor given by

$$T_{\text{fluid}}^{\mu\nu} = w u^\mu u^\nu - g^{\mu\nu} p, \quad (2.4)$$

where u^μ is the four-velocity of the plasma (normalized such that $u_\mu u^\mu = 1$), while p and w are respectively the pressure and the enthalpy density. Following [13, 16], we define the transition strength as the normalized difference of the so-called pseudotrace between the symmetric and broken phase

$$\alpha_{\bar{\theta}} = \frac{\Delta \bar{\theta}}{3w_s}, \quad \text{with} \quad \bar{\theta} = e - \frac{p}{c_b^2}, \quad (2.5)$$

where c_b is the speed of sound in the broken phase, while $e = w - p$ is the fluid energy density. Additionally, we use the ratio of enthalpy between broken and symmetric phases

$$\Psi = \frac{w_b}{w_s}. \quad (2.6)$$

Both $\alpha_{\bar{\theta}}$ and Ψ are evaluated at the nucleation temperature T_n .

3 Matching conditions beyond local thermal equilibrium

3.1 Stationary bubble-walls

Conservation of the energy-momentum tensor (2.4), together with the assumptions of the scale invariance and spherical symmetry of the solution leads to the following set of differential equations describing thermodynamical profiles of the plasma [33]

$$\begin{aligned} 2\frac{v}{\xi} &= \gamma^2(1 - v\xi) \left[\frac{\mu^2(\xi, v)}{c^2} - 1 \right] \partial_\xi v, \\ \partial_\xi w &= w \left(1 + \frac{1}{c^2} \right) \gamma^2 \mu \partial_\xi v, \end{aligned} \tag{3.1}$$

where the self-similar variable $\xi \equiv r/t$ is the distance from the bubble centre divided by the time elapsed since nucleation and c stands for the speed of sound. The plasma velocity v is defined in the reference frame of the bubble centre (also called plasma rest frame) and its Lorentz boost to the frame of the bubble wall is given by

$$\mu(\xi, v) \equiv \frac{\xi - v}{1 - \xi v}.$$

Boundary conditions, necessary to solve this system and obtain the profile of plasma velocity and enthalpy are derived from the conservation of the energy-momentum tensor across the wall

$$\partial_\mu T_{\text{fluid}}^{\mu\nu} = 0. \tag{3.2}$$

By integrating (3.2) over the bubble profile at steady state within the planar wall approximation, one obtains the two well-known matching conditions

$$w_+ \gamma_+^2 v_+ = w_- \gamma_-^2 v_-, \tag{3.3}$$

$$w_+ \gamma_+^2 v_+^2 + p_+ = w_- \gamma_-^2 v_-^2 + p_-, \tag{3.4}$$

where all thermodynamical quantities are evaluated respectively in front of (+) and behind (−) the wall. These conditions are obtained in the *reference frame of the bubble wall*, but we assume trivial transformation of entropy and pressure and therefore the w_\pm and p_\pm can be used also in the plasma rest frame. The resulting thermodynamical profiles constitute a family of solutions which can be parameterized with the transition strength α_θ and the bubble-wall velocity ξ_w (assuming $c_s^2 = c_b^2 = \frac{1}{3}$, however solutions can be easily generalized beyond the limit of the relativistic gas for the speed of sound, see [16, 35]). To eliminate one of them, an additional constraint is needed. Recently it was proposed [13, 16], that the conservation of entropy can be used, assuming the limit of local thermal equilibrium. The next section is devoted to our derivation of a more general form of this condition.

3.2 Third matching condition

The additional relation between the thermodynamic quantities in both phases can be derived by analysing the entropy production in the steady state of the system. We assume that the only process in which the entropy is produced during FOPT is a dissipative friction-like interaction of thermal plasma with the moving wall. This interaction depends on the

microscopic structure of the model, plasma velocity, field profile and temperature across the wall

$$\partial_\mu(u^\mu s) = f_s(v, \phi, T). \quad (3.5)$$

By integrating (3.5) over bubble wall *in the wall frame*, one obtains

$$\frac{\partial}{\partial t} \left(\int_M dV s \gamma \right) - \int_M dV (\nabla \cdot (s \gamma \vec{v})) = \int_M dV f_s(v, \phi, T), \quad (3.6)$$

where M is a thin shell with $\partial_r \phi \neq 0$. Assuming a steady state, the total amount of entropy in the bubble wall does not change and hence the time derivative of the total entropy vanishes. We use Gauss's theorem to trade volume integral over entropy current divergence for the flux through the boundaries of our region. In the planer wall limit, this condition reads

$$s_- \gamma_- v_- - s_+ \gamma_+ v_+ = \int_{z_-}^{z_+} dz f_s(v, \phi, T), \quad (3.7)$$

and the associated error is proportional to L_w/r which is tiny in realistic situations. This expression is identical to the familiar local thermal equilibrium condition [13, 16] after setting $f_s = 0$. The inhomogeneity given by the integral over field profile can be interpreted as the entropy production rate at the bubble-front and will be denoted with

$$\Delta S = \int_{z_-}^{z_+} dz f_s(v, \phi, T). \quad (3.8)$$

With the help of the definition of enthalpy $w = \frac{s}{T}$ and the matching condition (3.3), we find

$$\frac{T_+}{T_-} = \frac{\gamma_-}{\gamma_+} \left(1 + \frac{T_+ \Delta S}{w_+ \gamma_+ v_+} \right) \quad (3.9)$$

which is the generalised form of our third matching condition.

3.3 Entropy production details

To evaluate the integral in ΔS , one has to know the form of the entropy source f_s , or equivalently the friction force exerted by thermal plasma on the advancing wall. This force is predetermined by the microscopic structure of the plasma and to derive it one has to solve intricate Boltzman equations. This approach was used to derive the friction in the SM [22] and the Minimal Supersymmetric Standard Model [23], assuming small deflection from thermal equilibrium, which is valid for weak FOPTs.

In this paper we follow different path, assuming phenomenological ansatz [24, 27, 36] which was also widely used in lattice studies of this system [37–41]

$$f_s(v, \phi, T) = \frac{\eta}{T} (u^\mu \partial_\mu \phi)^2, \quad (3.10)$$

with a free parameter η encoding the microscopic model structure. The support of the scalar field derivative $\partial_\mu \phi$ is limited to the bubble front, and thus we can estimate ΔS by setting $1/T$ and $u^\mu u^\nu$ to their values in front of the bubble wall as

$$\Delta S \approx \frac{\eta}{T_+} u_+^\mu u_+^\nu \int_{z_-}^{z_+} dz \partial_\mu \phi \partial_\nu \phi. \quad (3.11)$$

To proceed further, one has to find the field profile. While this is not an easy task in general, here we use the hyperbolic tangent ansatz suitable for most physical cases. In the wall frame it reads

$$\phi(z, t) = \frac{v_0}{2} \left[1 - \tanh \left(\frac{z}{L_w} \right) \right], \quad (3.12)$$

Here v_0 is the scalar vacuum expectation value (VEV) at the broken phase and L_w is the field profile width measured in the wall frame. With the field profile (3.12) and the four-velocity of the perfect fluid $u = (\gamma, v\gamma, 0, 0)$, the integral (3.11) can be evaluated analytically, yielding

$$\frac{\eta(v_+ \gamma_+)^2}{T_+} \int_{z_-}^{z_+} dz (\partial_z \phi)^2 = \frac{\eta v_0^2}{3 L_w} \frac{\gamma_+^2 v_+^2}{T_+}, \quad (3.13)$$

where the integration limits were fixed as $z_- = -\infty$, $z_+ = +\infty$, since the derivative of the field profile $\partial_z \phi$ decreases fast away from M and thus the integration may be extended to the whole real domain.

After inserting (3.13) into (3.9), the third matching condition becomes

$$\frac{T_+}{T_-} = \frac{\gamma_-}{\gamma_+} (1 + \rho \gamma_+ v_+) \quad (3.14)$$

where we introduce the normalized friction parameter ρ , defined as

$$\rho \equiv \eta \frac{v_0^2}{3 w_+ L_w}. \quad (3.15)$$

Notice that in the limit $\eta \rightarrow 0$ one retrieves matching condition for the LTE regime [13, 16].

4 Analytical results

In this section, we solve the system (3.1) beyond LTE utilizing new matching condition (3.14) together with two old ones (3.3) and (3.4). The problem is handled with the modified `Python` code from [16], publicly available at [25].

The limiting case with $\rho \rightarrow 0$ corresponding to the LTE approximation is presented on the left panel of Fig. 1, where different types of stationary solutions are shown on the (α_θ, Ψ) plane. Region I corresponds to the stationary deflagration/hybrid solutions found in [16], while region III represents the runaway scenario. Note that contrary to the previous studies [13, 16], we found that in the part of the parameter space (region II), the non-zero value of the friction may lead to the existence of stable detonation solutions which in the limit $\rho \rightarrow 0$ become runaways¹. In such a case both runaway and deflagration/hybrid solutions are possible, however as we will show later in this paper, the faster solution is strongly preferred.

The whole ρ -dependent solution for a fixed value of Ψ is presented in the right panel of Fig. 1. The coloured lines indicate wall velocities with red ones corresponding to detonation

¹Reference [13] also finds detonation solutions for some benchmarks in LTE, but correctly classifies them as unphysical. Here, we found a different branch of stable detonation solutions, which do not exist in LTE. For all solutions on this new branch we find $\xi_w \rightarrow 1$ in the limit $\eta \rightarrow 0$ which corresponds to LTE.

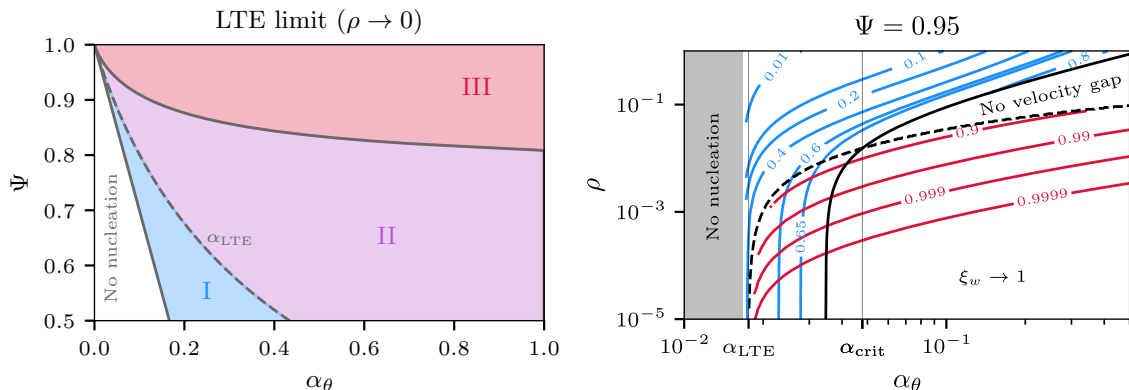


Figure 1. Bubble-wall velocity evaluated using the beyond LTE third matching condition (3.14) with $c_s^2 = c_b^2 = \frac{1}{3}$.

Left panel: LTE limit of the hydrodynamic solution. Region I corresponds to the case, when only deflagration/hybrid branch exists for $\rho \rightarrow 0$. Region II denotes the situation where both deflagration/hybrid and detonation branches coexist, however, the detonation solution is typically realized in lattice simulations. Region III corresponds to the situation with no deflagration/hybrid solution (runaway scenario).

Right panel: contour plot of the bubble wall velocity in (α_θ, ρ) plane for fixed $\Psi = 0.95$. The red contours represent detonation solutions with different values of the velocity, while deflagration/hybrid profiles are coloured in blue. Solid black line marks the contour of Jouguet deflagration, below which there is no stable deflagration or hybrid, while black dashed line limits the region where detonation solutions exist. For transitions with $\alpha < \alpha_{LTE}$, only deflagration/hybrid solutions exist in the limit of $\rho \rightarrow 0$. In the grey shaded region nucleation is forbidden.

solutions, while blue lines correspond to deflagration and hybrid solutions. The solid black line corresponds to the Jouguet velocity [16]

$$c_J \equiv c_b \left(\frac{1 + \sqrt{3\alpha_\theta(1 - c_b^2 + 3c_b^2\alpha_\theta)}}{1 + 3c_b^2\alpha_\theta} \right), \quad (4.1)$$

indicating the fastest deflagrations/hybrids, while the dashed black line shows where the slowest detonation solutions lie.

For typical phase transitions the LTE limit $\rho \rightarrow 0$ corresponding to the bottom of the plot leads to ultrarelativistic detonations with $\xi_w \rightarrow 1$, however for weaker transitions, deflagration and hybrid solutions can also be found. In the next sections, we will show that in the case where these solutions coexist, the faster detonation solution is typically realised. As the friction parameter grows, the wall velocity decreases and for detonation solutions it approaches the lower velocity limit denoted with black dashed line. When friction is even larger, we find only the deflagration/hybrid branch and the wall velocity continues to decrease with the increasing friction parameter.

For latent heat below the threshold value of the α_{crit} , the velocity of the slowest detonation is above c_J , while the corresponding deflagrations/hybrids crossing the dashed line are slower than c_J . Therefore, we find a gap in allowed velocities discussed in [26]. For

stronger transitions with $\alpha_\theta > \alpha_{\text{crit}}$, all the velocities are kinematically allowed and can be potentially realized ².

If the transition is sufficiently weak ($\alpha_\theta < \alpha_{\text{LTE}}$), only deflagration/hybrid solutions exist for any value of ρ . This region seems tiny, however becomes larger for lower values of Ψ (see the left panel). This situation corresponds to the real hydrodynamic obstruction [34], where pure equilibrium backreaction stops the acceleration. We believe that only in this weak transition regime the LTE estimate of the bubble-wall velocity [16] is realised. The value of α_{LTE} is determined numerically as the asymptotic behaviour of the black dashed curve for $\rho \rightarrow 0$. It corresponds to the dashed line between region I and II on the left panel of Fig. 1.

Even though, we expect that for ultrarelativistic walls our ansatz for the entropy source (3.10) could be inappropriate [33, 42], the results for detonations can be used to check if bubble wall reaches the deflagration/hybrid steady state or continues to accelerate. Clearly, for those benchmarks for which detonation solution does not exist regardless of η value, the walls cannot reach ultrarelativistic velocities, and the only possible solution type is deflagration or hybrid. Thus one obtains a simple condition for the validity of LTE predictions of the bubble wall velocities.

5 Hydrodynamic simulations

To verify the analytical predictions, we performed real-time simulations of the bubble growth.

Similarly as in [24, 36–41], we describe the plasma as a perfect fluid with temperature T , characterized by the internal energy density e , pressure p and enthalpy density w . As the effective potential $V_{\text{eff}}(\phi, T)$ can be interpreted as the free energy density \mathcal{F} of the system, we define the equation of state as

$$p(\phi, T) = -V_{\text{eff}}(\phi, T), \quad (5.1)$$

$$e(\phi, T) = V_{\text{eff}}(h, s, T) - T \frac{\partial V_{\text{eff}}(\phi, T)}{\partial T}, \quad (5.2)$$

$$w(\phi, T) = -T \frac{\partial V_{\text{eff}}(\phi, T)}{\partial T}. \quad (5.3)$$

The energy-momentum tensor of such a system is given by

$$T^{\mu\nu} = T_{\text{field}}^{\mu\nu} + T_{\text{fluid}}^{\mu\nu}, \quad (5.4)$$

where $T_{\text{fluid}}^{\mu\nu}$ is defined as in (2.4), while for the scalar field³

$$T_{\text{field}}^{\mu\nu} = \partial^\mu \phi \partial^\nu \phi - g^{\mu\nu} \left(\frac{1}{2} \partial_\alpha \phi \partial^\alpha \phi \right). \quad (5.5)$$

²Although our code [25] predicts a tiny gap between slowest detonation and Joguet velocity also for $\alpha_\theta > \alpha_{\text{crit}}$, the hydrodynamic simulations show that the transition between deflagration/hybrid and detonation branch is smooth.

³Note that in our convention the vacuum energy is a part of the fluid energy-momentum tensor and is not present here.

The energy-momentum tensor of the system is conserved ($\nabla_\mu T^{\mu\nu} = 0$), however, both contributions are not conserved separately

$$\nabla_\mu T_{\text{field}}^{\mu\nu} = -\nabla_\mu T_{\text{fluid}}^{\mu\nu} = \frac{\partial V}{\partial \phi} \partial^\nu \phi + \eta u^\mu \partial_\mu \phi \partial^\nu \phi, \quad (5.6)$$

where the right-hand side can be interpreted as the interaction between the plasma and the field, consisting of the equilibrium backreaction and the dissipative friction parametrized by η . In this approach the non-equilibrium part leads to the local production of entropy at the bubble front, as in (3.10).

Assuming spherical symmetry of the problem and introducing variables $Z := w\gamma^2 v$ and $\tau := w\gamma^2 - p$, we get in the plasma rest frame

$$-\partial_t^2 \phi + \frac{1}{r^2} \partial_r (r^2 \partial_r \phi) = \frac{\partial V_{\text{eff}}}{\partial \phi} + \eta \gamma (\partial_t \phi + v \partial_r \phi) \quad (5.7)$$

$$\partial_t \tau + \frac{1}{r^2} \partial_r (r^2 (\tau + p) v) = \frac{\partial V_{\text{eff}}}{\partial \phi} \partial_t \phi + \eta \gamma (\partial_t \phi + v \partial_r \phi) \partial_t \phi \quad (5.8)$$

$$\partial_t Z + \frac{1}{r^2} \partial_r (r^2 Z v) + \partial_r p = -\frac{\partial V_{\text{eff}}}{\partial \phi} \partial_r \phi - \eta \gamma (\partial_t \phi + v \partial_r \phi) \partial_r \phi. \quad (5.9)$$

This, together with the equations of state (5.1)–(5.3), define the dynamics of the system which we solve numerically on a lattice. We initialized each simulation with field profiles corresponding to the nucleated critical bubble, while plasma velocity and temperature were fixed as spatially uniform, $v(r) = 0$ and $T(r) = T_n$ respectively.

6 Numerical results

As a practical example, we will utilise the popular scalar singlet model (xSM) [43–59], although features we discuss are general and would carry over to many other extensions of the SM. We generalized the equation (5.7)–(5.9) for two fields $\phi = (h, s)$ (see [21]). Similarly as in [14, 15], we assume that the non-equilibrium friction is produced only through the coupling to the Higgs field, therefore from now on we assume $\eta_h = \eta$ and $\eta_s = 0$. For the details of the numerical treatment see Appendix A of [21].

As we already discussed, with the generalized third matching equation (3.14) we retrieve two types of steady-state solutions: deflagrations, whose wall velocity approaches the LTE prediction in the limit $\eta \rightarrow 0$ and stable detonations that for $\eta \rightarrow 0$ reach $\xi_w \rightarrow 1$. Here, for benchmark points representing both categories (see Table 1) we compare these analytical predictions with the results of the real-time simulations.

In order to translate the friction parameter η used in the hydrodynamic simulation into the normalised friction parameter value ρ , one needs to compute the width of the wall L_w for the stationary field profile. It is therefore crucial to learn how to predict the profile width at a steady state without solving the full system equations of motion. For this purpose, we use the simple analytical approximation

$$L_w \approx \frac{h_0}{\sqrt{2\Delta V_{\text{eff}}(T_n)}} \quad (6.1)$$

	α_θ	Ψ_n	$w_b(T_n)$ [GeV ⁴]	T_n [GeV]	h_0 [GeV]	L_w^{LTE} [GeV ⁻¹]
Benchmark 1	0.0072	0.972	2.94×10^9	96.8	172	0.198
Benchmark 2	0.0103	0.979	3.87×10^9	90.6	182	0.170

Table 1. Benchmark realisations of the $x\text{SM}$ model: **Benchmark 1** is an example of the model which evolves towards stationary subsonic deflagration in the limit of $\eta \rightarrow 0$. In the same limit **Benchmark 2** evolves as the ultra-relativistic detonation, although the analytical deflagration solution, predicted by the LTE equations, exists. The scan with respect to the friction parameter η is presented on Fig 2

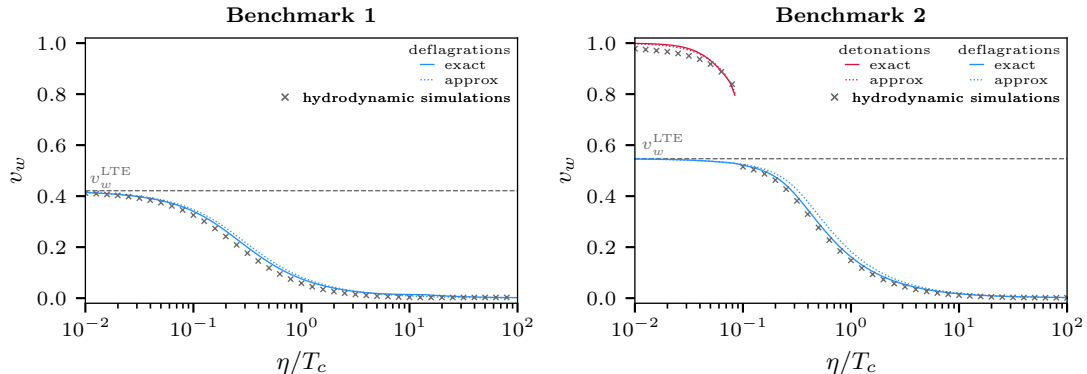


Figure 2. The bubble wall velocity v_w in the stationary state plotted against the effective friction parameter η for two benchmarks (see Table 1). Red and blue curves represent the analytical results with the third matching condition beyond LTE given with eq. (3.14). Solid and dotted lines denote different methods of bubble wall width evaluation: the exact value measured from the simulation, and the simple analytical approximation (6.1). Gray dashed lines mark the standard LTE analytical results (see [16]), while grey crosses represent the results of real-time lattice simulations with the full equations of motion of the system.

which depends only on the Higgs VEV h_0 and the potential difference between the supercooled and true vacua at the nucleation temperature. We will show this very simple expression is enough to give an accurate approximation of the wall velocity. In appendix A we motivate this expression and compare it with the profile widths obtained directly from results of lattice simulations. We also discuss the more involved formula which is usually slightly more precise, however, it requires the calculation of the tunnelling path in the field space.

Fig. 2 shows our predictions for the terminal wall velocity with the friction coupling η treated as a free parameter and probed throughout several orders of magnitude. Grey crosses show the values computed directly from the simulation. Our steady-state asymptotic predictions, determined with extended matching conditions at different η are plotted with lines. The deflagration/hybrid branch of solutions is denoted with blue, while the detonation branch is in red, similar to Fig. 1. The solid lines show our analytical estimates discussed in Sec. 3 with the wall width from the simulation used in Eq. (3.15), while to compute the dashed lines we use the simple approximation for the width from Eq. (6.1) instead. We can see that the uncertainty associated with that simple estimate is very small. The horizontal

grey dashed line shows the velocity in the LTE limit.

The left panel represents the benchmark with $\alpha_\theta < \alpha_{\text{LTE}}$, where in the LTE limit hydrodynamic obstruction stops the acceleration and the stationary state is achieved. The right panel corresponds to the benchmark with $\alpha_\theta > \alpha_{\text{LTE}}$, for which two distinct steady-states are kinematically allowed. When there is more than one stable asymptotic solution for the PDE, it is the initial state that determines which of the steady states is realised. Starting with the nucleating bubble, our simulations show it is the faster solution that is strongly preferred. The reason is that the fluid shell is still forming when the wall accelerates past the slower solution's velocity and the friction profile at the time does not resemble the asymptotic one that analytical methods assume ⁴.

7 Conclusions

In this work, we investigate the possible hydrodynamic solutions for a steady-state bubble wall in cosmological phase transitions. We extend the analytical computation based on thin wall approximation with the matching condition describing the entropy production in order to predict the wall velocity. This allows us to show that there is a new branch of solutions consisting of stable detonations which in the limit of vanishing friction would correspond to runaway solutions. We also show how a simple ansatz for the phenomenological friction parameter often used in lattice realisations is tied to entropy production at the bubble wall. We provide a modified version of the `Python` code developed for the local thermal equilibrium case [16] which allows one to find the non-equilibrium solutions given the phenomenological friction [25].

Next, we use real-time lattice simulations starting from nucleating bubble solutions to verify our results. We find our analytical solutions to match the lattice simulation results very well. The matching also requires an estimate of the width of the wall. We provide simple approximations for the width which require only the knowledge of the potential and the temperature and demonstrate they are accurate despite their simplicity.

This allows us to predict the character of solutions in the entire parameter space of models. We find that above the critical value for the phase transition strength, there is no gap between the velocities of the two branches of solutions and in principle all the profiles are kinematically allowed. We also show that below that critical value, the deflagration/hybrid solutions often coexist with the new detonation branch, however, there is a velocity gap between the two. Most importantly using our real-time simulations we show that it is the faster detonation solution which will be realised in such cases. The reason behind this is that in analytical methods we assume a fully developed steady-state thermodynamically profile for all solutions. In simulations, we see that the plasma shell is typically still forming and exerts much smaller friction as the wall accelerates past the slower solution.

⁴We discussed the same issue in LTE with $\eta = 0$ in ref. [21] where walls would accelerate past the deflagration/hybrid LTE solutions and run away.

Acknowledgements

We would like to acknowledge Bogumiła Świeżewska, José Miguel No and Marcin Badziak for the discussion on the draft. ML and MZ were supported by the Polish National Agency for Academic Exchange within Polish Returns Programme under agreement PPN/PPO/2020/1/00013/U/00001 and the Polish National Science Centre grant 2018/31/D/ST2/02048. IN was partially supported by the National Science Centre, Poland, under research grant no. 2020/38/E/ST2/00243. TK was supported by Polish National Science Centre grant 2019/33/B/ST9/01564. MZ and IN were also supported with the IDUB Early Universe scholarships.

A Field profile widths

In this appendix, we discuss steady-state field profiles across the wall. We begin by deriving the equation for steady profiles in the wall frame. Next, we impose the hyperbolic tangent ansatz

$$\phi_i = \frac{v_i}{2} \left[1 \pm \tanh \left(\frac{z - \delta_i}{L_i} \right) \right] \quad (\text{A.1})$$

with some specific width L_i and displacement δ_i from the centre of the wall⁵ for each field that participates in tunnelling during the FOPT. We substitute the ansatz (A.1) to the equation for steady profiles and find approximate expressions for the profile widths L_i . Finally, we use these expressions to compute the wall width in the xSM and compare the outcome with the results of hydrodynamic simulations.

A.1 Equation for steady profiles

We begin from the scalar field EOM (5.7) written in the planar wall limit

$$-\partial_t^2 \phi + \partial_z^2 \phi - \frac{\partial V_{\text{eff}}}{\partial \phi} = \eta \gamma (\partial_t \phi + v \partial_z \phi) \quad (\text{A.2})$$

where ϕ could be a single field or a vector of dynamical scalar fields, that tunnel through the potential barrier. We neglected the effects of the wall curvature since the associate error is proportional to the inverse of the bubble radius and should be negligible in late stages of its evolution.

To get the equation for a steady profile in the wall frame, we set all time derivatives of the fields to zero. The lattice simulation results indicate that the field profiles weakly depend on η (see the right panel in Fig. 3) and therefore we can safely neglect the friction term, at least for deflagrations/hybrids. The resulting equation

$$\partial_z^2 \phi - \frac{\partial V_{\text{eff}}}{\partial \phi} = 0, \quad (\text{A.3})$$

is equivalent to the classical equation of motion of a particle with “position” ϕ , “time” z and “potential” $-V(\phi, T(z))$. The potential depends on the “time” z through the temperature,

⁵For a sufficiently long evolution of the bubble, its wall becomes arbitrarily thin compared to the plasma profile. In this limit the notion of the bubble wall centre is ambiguous. Therefore, one can pick any field profile to be “central” and offset its δ from other profile displacements.

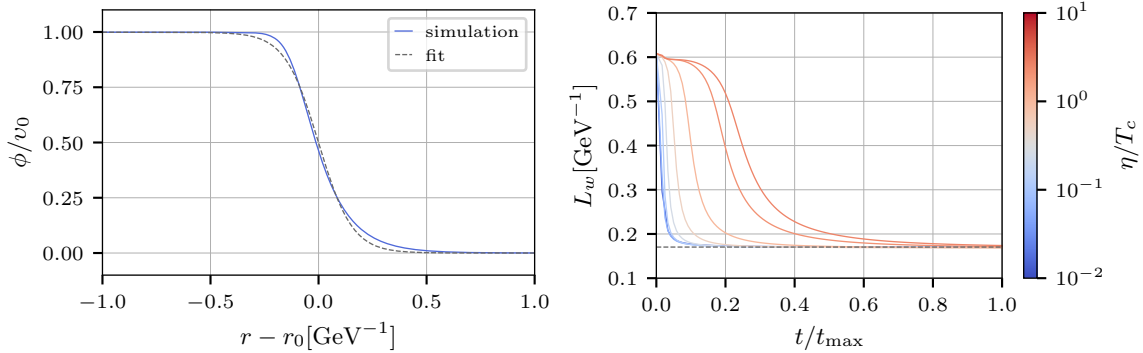


Figure 3. Left panel: example of the field profile from the real-time simulation at its final time $t = t_{max}$ compared with the fit given with eq. (3.12). The resulting L_w was used to determine ρ with eq. (3.15). Right panel: time evolution of L_w for **Benchmark 1** (see Table 1). Different colours represent different values of the effective friction parameter η . The asymptotic value L_w^{LTE} is achieved in the whole spectrum of η values.

whose profile across the rarefaction front cannot be found without solving the steady-state equations of motion for the plasma. Despite this, for the transitions with $T_n \sim T_c$ (which is always fulfilled for the xSM deflagrations/hybrids in the LTE limit [21]) the temperature does not change much across the wall, and the precise estimate of the field profile is obtained by solving (A.3) at the critical temperature

$$\partial_z^2 \phi = \frac{\partial V_{\text{eff}}(\phi, T = T_c)}{\partial \phi}. \quad (\text{A.4})$$

This equation can be integrated numerically, with ϕ equal to the symmetric and broken VEVs at $z = \pm\infty$, but the resulting boundary value problem is still demanding. In the next section, we use equation (A.4) to derive simple approximations for the profile width L_w , applicable to a wide class of models and show their excellent accuracy.

A.2 Approximate solutions for profile width

The potential in (A.4) does not explicitly depend on “time” z , thus the equation has energy-like integral of motion

$$\frac{(\partial_z \phi)^2}{2} = V_{\text{eff}}(\phi) - V_{\text{eff}}(\phi|_{\pm\infty}). \quad (\text{A.5})$$

For a single-field problem, this equation is sufficient to get the profile width. After substituting hyperbolic tangent ansatz (A.1) to (A.5) and setting $z = 0$ one obtains [60]

$$L_w = \frac{v_0}{\sqrt{8V_b}}, \quad (\text{A.6})$$

where v_0 is the scalar VEV at broken vacuum, while V_b is the barrier height. When there are many dynamical fields whose profiles do not overlap, one can assume, that at the centre of each field profile its “kinetic” term $(\partial_z \phi_i)^2/2$ dominates other derivative terms in (A.5). The multi-field variant of the approximation (A.6) is very precise, provided one uses the correct value for the potential barrier, which should be the maximal potential value *on the*

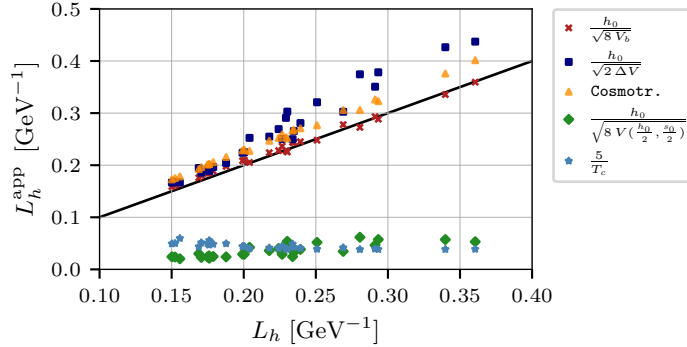


Figure 4. Different approximations for the Higgs field profile width at the steady state L_h^{app} , plotted against values obtained in lattice simulations L_h .

tunnelling path⁶. Alternatively, one can use an approximate relation that holds for 1D transitions

$$V_b(T_c) \approx \frac{1}{4} \Delta V_{\text{eff}}(T_n), \quad (\text{A.7})$$

where $\Delta V(T_n)$ is a difference between the effective potential taken in a broken and symmetric vacua at the nucleation temperature. Since the computation of $\Delta V(T_n)$ does not require knowledge of the tunnelling path, one can substitute it into (A.6), obtaining simple and model agnostic estimate

$$L_w \approx \frac{v_0}{\sqrt{2\Delta V_{\text{eff}}}}.$$

A.3 Comparison with simulation results

In the xSM precise values of the wall width can be obtained by fitting hyperbolic tangent as given by eq. (3.12) to the field profile obtained in the lattice simulations. Example of such a fit is shown in the left panel of Fig. 3, while in the right panel, we present the time evolution of the fitted wall width towards the stationary limit. Crucially, within the deflagration/hybrid branch, the asymptotic value of L_w does not depend on the effective friction η , which justifies neglecting the friction term in (A.2). We find that regardless of the method used for L_w computation our asymptotic approach is surprisingly accurate.

We use the fitted value of L_w to assess analytical expressions (A.6) and (6.1) as well as other estimates proposed in the literature [11, 52, 60, 61]. The resulting comparison is shown in Fig. 4. While all the analysed methods correctly predict the order of magnitude of L_h , exact values often differ significantly from lattice results. The most precise predictions, within 6% from the lattice, were obtained with (A.6) where V_b was evaluated on the tunnelling path. The naive estimate (6.1), was found surprisingly accurate for smaller profile widths, but for larger L_h it overshoots the lattice results by up to 35%. In our comparison, we also include the build-in `Cosmotransitions` routine for finding the profile of the wall

⁶The tunnelling path in the vicinity of the critical temperature can be easily estimated with the routine provided by `Cosmotransitions` package.

moving through the plasma⁷ (not to be confused with the routine computing the critical profile). This method also overshoots the lattice values, but the results are within 15% from the full solutions of the EOM. A simple estimate that assumes a symmetric barrier

$$L_h \approx \frac{h_0}{\sqrt{8V_{\text{eff}}(\frac{h_0}{2}, \frac{s_0}{2})}},$$

predicts L_h to be 5 to 8 times smaller than the corresponding profile widths obtained on the lattice. Also the approximation based on the critical temperature:

$$L_h \approx \frac{5}{T_c},$$

significantly underestimates the widths of the xSM Higgs profiles.

References

- [1] V.A. Kuzmin, V.A. Rubakov and M.E. Shaposhnikov, *On the Anomalous Electroweak Baryon Number Nonconservation in the Early Universe*, *Phys. Lett. B* **155** (1985) 36.
- [2] A.G. Cohen, D.B. Kaplan and A.E. Nelson, *Progress in electroweak baryogenesis*, *Ann. Rev. Nucl. Part. Sci.* **43** (1993) 27 [[hep-ph/9302210](#)].
- [3] V.A. Rubakov and M.E. Shaposhnikov, *Electroweak baryon number nonconservation in the early universe and in high-energy collisions*, *Usp. Fiz. Nauk* **166** (1996) 493 [[hep-ph/9603208](#)].
- [4] D.E. Morrissey and M.J. Ramsey-Musolf, *Electroweak baryogenesis*, *New J. Phys.* **14** (2012) 125003 [[1206.2942](#)].
- [5] C. Caprini et al., *Science with the space-based interferometer eLISA. II: Gravitational waves from cosmological phase transitions*, *JCAP* **04** (2016) 001 [[1512.06239](#)].
- [6] C. Caprini et al., *Detecting gravitational waves from cosmological phase transitions with LISA: an update*, *JCAP* **03** (2020) 024 [[1910.13125](#)].
- [7] L. Badurina, O. Buchmueller, J. Ellis, M. Lewicki, C. McCabe and V. Vaskonen, *Prospective sensitivities of atom interferometers to gravitational waves and ultralight dark matter*, *Phil. Trans. A. Math. Phys. Eng. Sci.* **380** (2021) 20210060 [[2108.02468](#)].
- [8] LISA COSMOLOGY WORKING GROUP collaboration, *Cosmology with the Laser Interferometer Space Antenna*, *Living Rev. Rel.* **26** (2023) 5 [[2204.05434](#)].
- [9] LISA COSMOLOGY WORKING GROUP collaboration, *Gravitational waves from first-order phase transitions in LISA: reconstruction pipeline and physics interpretation*, *JCAP* **10** (2024) 020 [[2403.03723](#)].
- [10] C. Caprini, O. Pujolàs, H. Quequejaya-Leclere, F. Rompineve and D.A. Steer, *Primordial gravitational wave backgrounds from phase transitions with next generation ground based detectors*, [2406.02359](#).

⁷The routine numerically solves the equation (A.3) at the nucleation temperature by adjusting η so that the field, rolling down from the global maximum of $-V_{\text{eff}}$ (true vacuum), stops exactly at the local maximum (false vacuum).

- [11] B. Laurent and J.M. Cline, *Fluid equations for fast-moving electroweak bubble walls*, *Phys. Rev. D* **102** (2020) 063516 [[2007.10935](#)].
- [12] M. Barroso Mancha, T. Prokopec and B. Swiezevska, *Field-theoretic derivation of bubble-wall force*, *JHEP* **01** (2021) 070 [[2005.10875](#)].
- [13] W.-Y. Ai, B. Garbrecht and C. Tamarit, *Bubble wall velocities in local equilibrium*, *JCAP* **03** (2022) 015 [[2109.13710](#)].
- [14] J.M. Cline, A. Friedlander, D.-M. He, K. Kainulainen, B. Laurent and D. Tucker-Smith, *Baryogenesis and gravity waves from a UV-completed electroweak phase transition*, *Phys. Rev. D* **103** (2021) 123529 [[2102.12490](#)].
- [15] B. Laurent and J.M. Cline, *First principles determination of bubble wall velocity*, *Phys. Rev. D* **106** (2022) 023501 [[2204.13120](#)].
- [16] W.-Y. Ai, B. Laurent and J. van de Vis, *Model-independent bubble wall velocities in local thermal equilibrium*, *JCAP* **07** (2023) 002 [[2303.10171](#)].
- [17] M. Sanchez-Garitaonandia and J. van de Vis, *Prediction of the bubble wall velocity for a large jump in degrees of freedom*, *Phys. Rev. D* **110** (2024) 023509 [[2312.09964](#)].
- [18] A. Ekstedt, O. Gould, J. Hirvonen, B. Laurent, L. Niemi, P. Schicho et al., *How fast does the WallGo? A package for computing wall velocities in first-order phase transitions*, [2411.04970](#).
- [19] W.-Y. Ai, B. Laurent and J. van de Vis, *Bounds on the bubble wall velocity*, [2411.13641](#).
- [20] T. Krajewski, M. Lewicki, M. Vasar, V. Vaskonen, H. Veermäe and M. Zych, *Thermalization effects on the dynamics of growing vacuum bubbles*, [2411.15094](#).
- [21] T. Krajewski, M. Lewicki and M. Zych, *Bubble-wall velocity in local thermal equilibrium: hydrodynamical simulations vs analytical treatment*, *JHEP* **05** (2024) 011 [[2402.15408](#)].
- [22] G.D. Moore and T. Prokopec, *How fast can the wall move? A Study of the electroweak phase transition dynamics*, *Phys. Rev. D* **52** (1995) 7182 [[hep-ph/9506475](#)].
- [23] P. John and M.G. Schmidt, *Do stops slow down electroweak bubble walls?*, *Nucl. Phys. B* **598** (2001) 291 [[hep-ph/0002050](#)].
- [24] J. Ignatius, K. Kajantie, H. Kurki-Suonio and M. Laine, *The growth of bubbles in cosmological phase transitions*, *Phys. Rev. D* **49** (1994) 3854 [[astro-ph/9309059](#)].
- [25] <https://github.com/wedelfach/Bubbles-beyond-LTE.git>.
- [26] T. Krajewski, M. Lewicki and M. Zych, *Hydrodynamical constraints on the bubble wall velocity*, *Phys. Rev. D* **108** (2023) 103523 [[2303.18216](#)].
- [27] S. Balaji, M. Spannowsky and C. Tamarit, *Cosmological bubble friction in local equilibrium*, *JCAP* **03** (2021) 051 [[2010.08013](#)].
- [28] S.R. Coleman, *The Fate of the False Vacuum. 1. Semiclassical Theory*, *Phys. Rev. D* **15** (1977) 2929.
- [29] C.G. Callan, Jr. and S.R. Coleman, *The Fate of the False Vacuum. 2. First Quantum Corrections*, *Phys. Rev. D* **16** (1977) 1762.
- [30] A.D. Linde, *Fate of the False Vacuum at Finite Temperature: Theory and Applications*, *Phys. Lett. B* **100** (1981) 37.

- [31] A.D. Linde, *Decay of the False Vacuum at Finite Temperature*, *Nucl. Phys. B* **216** (1983) 421.
- [32] J. Ellis, M. Lewicki and J.M. No, *On the Maximal Strength of a First-Order Electroweak Phase Transition and its Gravitational Wave Signal*, *JCAP* **04** (2019) 003 [[1809.08242](#)].
- [33] J.R. Espinosa, T. Konstandin, J.M. No and G. Servant, *Energy Budget of Cosmological First-order Phase Transitions*, *JCAP* **06** (2010) 028 [[1004.4187](#)].
- [34] T. Konstandin and J.M. No, *Hydrodynamic obstruction to bubble expansion*, *JCAP* **02** (2011) 008 [[1011.3735](#)].
- [35] F. Giese, T. Konstandin, K. Schmitz and J. van de Vis, *Model-independent energy budget for LISA*, *JCAP* **01** (2021) 072 [[2010.09744](#)].
- [36] H. Kurki-Suonio and M. Laine, *On bubble growth and droplet decay in cosmological phase transitions*, *Phys. Rev. D* **54** (1996) 7163 [[hep-ph/9512202](#)].
- [37] M. Hindmarsh, S.J. Huber, K. Rummukainen and D.J. Weir, *Gravitational waves from the sound of a first order phase transition*, *Phys. Rev. Lett.* **112** (2014) 041301 [[1304.2433](#)].
- [38] M. Hindmarsh, S.J. Huber, K. Rummukainen and D.J. Weir, *Numerical simulations of acoustically generated gravitational waves at a first order phase transition*, *Phys. Rev. D* **92** (2015) 123009 [[1504.03291](#)].
- [39] M. Hindmarsh, S.J. Huber, K. Rummukainen and D.J. Weir, *Shape of the acoustic gravitational wave power spectrum from a first order phase transition*, *Phys. Rev. D* **96** (2017) 103520 [[1704.05871](#)].
- [40] D. Cutting, M. Hindmarsh and D.J. Weir, *Vorticity, kinetic energy, and suppressed gravitational wave production in strong first order phase transitions*, *Phys. Rev. Lett.* **125** (2020) 021302 [[1906.00480](#)].
- [41] D. Cutting, E. Vilhonen and D.J. Weir, *Droplet collapse during strongly supercooled transitions*, *Phys. Rev. D* **106** (2022) 103524 [[2204.03396](#)].
- [42] D. Bodeker and G.D. Moore, *Can electroweak bubble walls run away?*, *JCAP* **05** (2009) 009 [[0903.4099](#)].
- [43] J. McDonald, *Electroweak baryogenesis and dark matter via a gauge singlet scalar*, *Phys. Lett. B* **323** (1994) 339.
- [44] J.R. Espinosa and M. Quiros, *The Electroweak phase transition with a singlet*, *Phys. Lett. B* **305** (1993) 98 [[hep-ph/9301285](#)].
- [45] J.R. Espinosa and M. Quiros, *Novel Effects in Electroweak Breaking from a Hidden Sector*, *Phys. Rev. D* **76** (2007) 076004 [[hep-ph/0701145](#)].
- [46] S. Profumo, M.J. Ramsey-Musolf and G. Shaughnessy, *Singlet Higgs phenomenology and the electroweak phase transition*, *JHEP* **08** (2007) 010 [[0705.2425](#)].
- [47] J.R. Espinosa, T. Konstandin and F. Riva, *Strong Electroweak Phase Transitions in the Standard Model with a Singlet*, *Nucl. Phys. B* **854** (2012) 592 [[1107.5441](#)].
- [48] V. Barger, D.J.H. Chung, A.J. Long and L.-T. Wang, *Strongly First Order Phase Transitions Near an Enhanced Discrete Symmetry Point*, *Phys. Lett. B* **710** (2012) 1 [[1112.5460](#)].
- [49] J.M. Cline and K. Kainulainen, *Electroweak baryogenesis and dark matter from a singlet Higgs*, *JCAP* **01** (2013) 012 [[1210.4196](#)].

- [50] T. Alanne, K. Tuominen and V. Vaskonen, *Strong phase transition, dark matter and vacuum stability from simple hidden sectors*, *Nucl. Phys. B* **889** (2014) 692 [[1407.0688](#)].
- [51] D. Curtin, P. Meade and C.-T. Yu, *Testing Electroweak Baryogenesis with Future Colliders*, *JHEP* **11** (2014) 127 [[1409.0005](#)].
- [52] V. Vaskonen, *Electroweak baryogenesis and gravitational waves from a real scalar singlet*, *Phys. Rev. D* **95** (2017) 123515 [[1611.02073](#)].
- [53] G. Kurup and M. Perelstein, *Dynamics of Electroweak Phase Transition In Singlet-Scalar Extension of the Standard Model*, *Phys. Rev. D* **96** (2017) 015036 [[1704.03381](#)].
- [54] A. Beniwal, M. Lewicki, J.D. Wells, M. White and A.G. Williams, *Gravitational wave, collider and dark matter signals from a scalar singlet electroweak baryogenesis*, *JHEP* **08** (2017) 108 [[1702.06124](#)].
- [55] A. Beniwal, M. Lewicki, M. White and A.G. Williams, *Gravitational waves and electroweak baryogenesis in a global study of the extended scalar singlet model*, *JHEP* **02** (2019) 183 [[1810.02380](#)].
- [56] L. Niemi, P. Schicho and T.V.I. Tenkanen, *Singlet-assisted electroweak phase transition at two loops*, *Phys. Rev. D* **103** (2021) 115035 [[2103.07467](#)].
- [57] J. Ellis, M. Lewicki, M. Merchand, J.M. No and M. Zych, *The scalar singlet extension of the Standard Model: gravitational waves versus baryogenesis*, *JHEP* **01** (2023) 093 [[2210.16305](#)].
- [58] M. Lewicki, M. Merchand, L. Sagunski, P. Schicho and D. Schmitt, *Impact of theoretical uncertainties on model parameter reconstruction from GW signals sourced by cosmological phase transitions*, *Phys. Rev. D* **110** (2024) 023538 [[2403.03769](#)].
- [59] O. Gould and P. Saffin, *Perturbative gravitational wave predictions for the real-scalar extended Standard Model*, [2411.08951](#).
- [60] S.J. Huber and M. Sopena, *An efficient approach to electroweak bubble velocities*, [1302.1044](#).
- [61] M. Lewicki, M. Merchand and M. Zych, *Electroweak bubble wall expansion: gravitational waves and baryogenesis in Standard Model-like thermal plasma*, *JHEP* **02** (2022) 017 [[2111.02393](#)].